Chinese Chemical Letters 33 (2022) 3259–3262

Contents lists available at ScienceDirect

Chinese Chemical Letters

journal homepage: www.elsevier.com/locate/cclet

In situ thermal-induced generation of $\{Ag^0Ag^I\}$ dimer within Co-Ag phosphonates

Qingqing Guo, Nanzhu Li, Qian Zou, Jiage Jia, Yifan Wei, Songsong Bao*, Limin Zheng

State Key Laboratory of Coordination Chemistry, School of Chemistry and Chemical Engineering, Collaborative Innovation Center of Advanced Microstructures, Nanjing University, Nanjing 210023, China

ARTICLE INFO

Article history:
Received 4 August 2021
Revised 21 October 2021
Accepted 31 October 2021
Available online 6 November 2021

Keywords:
Metallic silver
Thermal decomposition
Metal phosphonate
Atomic dispersion
Magnetism

ABSTRACT

The thermal decomposition of $AgNO_3$ is known to produce metallic Ag, but single-atomic dispersion is hard to achieve instead of the aggregation state of nanoparticles. Herein, we develop an efficient approach to thermally generate and stabilize single Ag atoms *via* the coordination effect. Two desired Co-Ag phosphonates $[Ag^I_2Co^{III}_2(notpH_3)_2(NO_3)]X$ [X = NO_3^- (**1**) or ClO_4^- (**2**)] were synthesized by solid-phase grinding method or solution crystallization. Both crystal structures reveal slightly different packing arrangements of various lattice anions and identical one-dimensional (1-D) coordination chains, formed in each case by the coordination of Ag(I) to the metalloligand $Co(notpH_3)$ and NO_3^- anion. The number of Ag(I) ions connected to each NO_3^- anion reduces from 5 in bulk $AgNO_3$ to 2 in compounds **1** and **2**, leading to the $AgNO_3$ component stepwise decomposition at a lower temperature (<300 °C). During the thermal decomposition, the changes of supermolecular structures and Ag oxidation states were monitored by PXRD, IR and XAFS measurements. The most interesting finding is that **1** and **2** can retain chain structures and harvest Ag(0) atoms in the chain by controlling decomposition temperatures (220 °C for **1** and 254 °C for **2**).

Coordination polymers (CPs) or metal-organic frameworks (MOFs) are periodic structures containing metal entities linked by organic ligands [1–3]. Due to the nature of metal centers' monodisperse and volatile metal oxidation state tuned by ligand coordination, CPs or MOFs provide a promising platform for designing single-atom materials (SAMs), applying in such as catalyst [4–11], battery [12] and solar cell [13]. The active metal sites can be introduced in pristine CPs or MOFs during a synthetic process or be in-situ produced in their derived materials under suitable thermal or chemical conversion processes [5,14,15]. In addition, isolated monometallic active sites can be constructed and further immobilized through the post-modification of metal nodes [4,16], organic ligands [17], or guest spaces [8]. However, it is still challenging to anchor single zero-valent metal atoms in CPs/MOFs and their derivatives, concerning the aggregation of metal atoms to nanoparticles and the optimal coordination geometry.

Metallic Ag nanoparticles (NPs) loaded materials have promising catalytic activities for photocatalytic water reduction and three-phase alkyne hydrogenation [18]. To promote photocatalytic performance, downsizing Ag NPs to Ag clusters or single-atom dispersion is expected to be a good strategy [10]. Recently, a few works were reported to anchor single Ag atoms in inorganic supports such as carbon nitride and MnO_x by coordination and achieving high stabilities and catalytic activities [18–23]. While the CPs/MOFs support can immobilize Ag NPs in a few cases [15,17], the observation of isolated single atoms of metallic silver in them is still rare.

The thermal decomposition of silver nitrate is well known to obtain metallic Ag, NO_2, and O_2. The resulting Ag(0) atoms usually aggregate and can be a precursor to synthesize the Ag NPs. We conjecture that Ag(0) atoms would be trapped in coordination spheres and atomically dispersed when $AgNO_3$ thermally decomposes in CPs/MOFs. To obtain such a compound is trouble in the combination of NO_3^- and a ligand within the same coordination sphere of Ag(I). In our previous work, the neutral mononuclear complex $Co(notpH_3)$ [$notpH_6$ = 1,4,7-triazacyclononane-1,4,7-triyl-tris(methylene-phosphonic acid)] can serve as a bi-, tri- or tetra-dentate metalloligand to ligate various metal cations [24–28]. Herein, we report two new $Co(notpH_3)$ based one-dimensional Co-Ag coordination polymers $[Ag^I_2Co^{III}_2(notpH_3)_2(NO_3)](NO_3)$ (**1**) and $[Ag^I_2Co^{III}_2(notpH_3)_2(NO_3)](ClO_4)$ (**2**). Compound **1** can be synthesized by simply grinding the mixture of $Co(notpH_3)$ and $AgNO_3$ solid (Fig. 1a). Each coordinated NO_3^- anion bridges two Ag(I) ions within the chains in both η^2- and η^1-forms.

* Corresponding author.
E-mail address: baososo@nju.edu.cn (S. Bao).

https://doi.org/10.1016/j.cclet.2021.10.091
1001-8417/

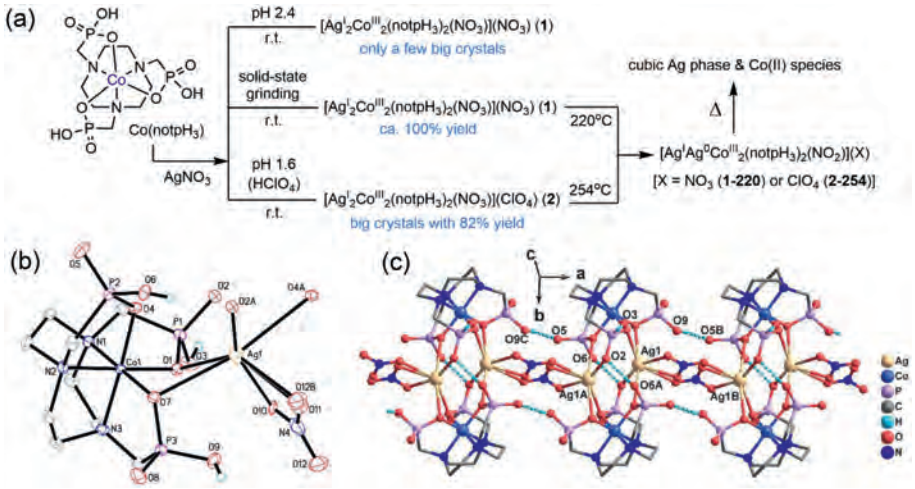

Fig. 1. (a) The synthetic route and decomposition of Co-Ag phosphonates. The diagrams show the asymmetric unit (b) and the coordination chain (c) of compound **1**. The disordered lattice NO_3^- anion and all H atoms except bonding to O3, O6 and O9 atoms are omitted for clarity. Symmetric operation: A −x, 1−y, −z; B 1−x, 1−y, −z; C −1 + *y*, y, z.

Interestingly, the thermal decomposition of $AgNO_3$ occurs in both compounds under lower temperatures compared to bulk $AgNO_3$. Moreover, the stepwise mass losses agree with the successive release of O_2 and NO_2. After heating at 220 °C for **1** and 254 °C for **2**, the intermediates exhibit invariable PXRD patterns and change from diamagnetism to two spin-1/2 paramagnetism. It indicates that the generating Ag(0) atoms (spin-1/2) and NO_2 (spin-1/2) molecules anchor in the coordination chains.

Single crystal X-ray structural analyses revealed that **1** crystallizes in the monoclinic $P2_1/n$ space group. The asymmetric unit consists of one Co(III), one Ag(I), one notpH$_3^{3-}$, a half coordination NO_3^-, and a half lattice NO_3^-. As shown in Fig. 1b, the Co(III) ion in the Co(notpH$_3$) adopts octahedral geometry, with three donor N atoms and three donor O atoms [Co-O: 1.921(2)–1.939(2) Å, Co-N: 1.933(3)–1.947(3) Å]. Each Ag(I) ion is coordinated by four O atoms (O1, O7, O2A, and O4A) from two Co(notpH$_3$) and one or two O atoms (O12B or O10 and O11) from disordered NO_3^- anions [Ag-O: 2.375(2)–2.859(3) Å]. The Ag1-O4A and Ag1-O7 bonds show long distances of 2.770(3) and 2.859(3) Å [29], but shorter than the sum of the van der Waals radii of ~3.7 Å [30]. Three O atoms (O3, O6, and O9) are protonated in Co(notpH$_3$), which serves as a tetra-dentate neutral metalloligand binding two equivalent Ag(I) ions [Ag1···Ag1A, 3.2384(7) Å] (Fig. 1c). The {Co_2Ag_2} units are fused by NO_3^- through its three O atoms [Ag1···Ag1B, 6.0822(9) Å], forming a one-dimensional (1-D) infinite chain along *a*-axis. Such an alternative chain structure bridged by two kinds of ligands is also observed in some 1-D metal chains [31–33]. Furthermore, the 1-D chain is stabilized through intrachain hydrogen-bonding interactions [34,35]. Each Co(notpH$_3$) servers as not only a hydrogen bond donor but also a hydrogen bond acceptor to connect the other three Co(notpH$_3$) within the chain [O6-H···O2A and O6A-H···O2: 2.613(3) Å; O9-H···O5C and O9B-H···O5: 2.541(3) Å]. The 1-D chains are packed into a 3-D supramolecular network through strong interchain hydrogen bonding [O3-H···O8D: 2.484(3) Å (symmetric code D, x, 0.5−y, −0.5 + *z*)] (Fig. S2a in Supporting information). The positive network is balanced by heavily disordered lattice NO_3^- anions.

Like **1**, compound **2** also crystallizes in the monoclinic $P2_1/n$ space group and has a similar asymmetric unit except that a half lattice ClO_4^- anion replaces a half lattice NO_3^- anion. ClO_4^- anions in the lattice have minimal impact on the coordination sphere, the chain's structure, and the H-bonding interactions between chains (Table S2, Figs. S2b and S3 in Supporting information). The smaller Ag···Ag distances of 3.189(3) Å within {Co_2Ag_2} units and of 6.062(4) Å between {Co_2Ag_2} units are observed in **2** probably due to the data collection at 173 K. The ClO_4^- anion in the lattice has a different shape from the NO_3^- anion, slightly changing the placement of coordination chains along *b* and *c* directions [β-angle: 96.196(3)° in **1** and 94.743(11)° in **2**].

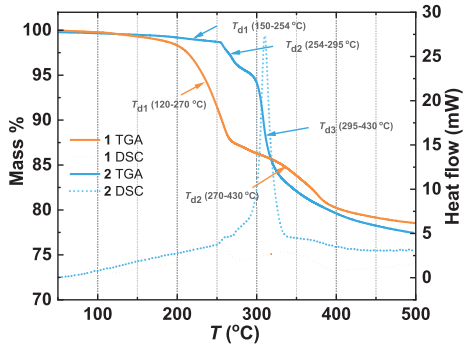

Fig. 2. Thermal stability of **1** and **2** under Ar atmosphere.

As expected, the $AgNO_3$ component homogeneously dispersed in hydrogen-bonded networks consist of cobalt phosphonates. The thermal stability of compounds **1** and **2** was determined by thermogravimetric (TG) analysis (Fig. 2). **1** was pre-dried under 120 °C to remove the absorbed water molecules in agglomerated particles of the wet-grinding synthesized sample. Both **1** and **2** have similar coordination chain structures and hydrogen-bonded networks. However, various lattice anions (NO_3^- in **1** and ClO_4^- in **2**) significantly affect thermal stability showing the different decomposition temperatures (T_d). We speculate that the size and geometry differences between NO_3^- and ClO_4^- could affect the thermal stability of **1** and **2**. The thermochemical radii of NO_3^- and ClO_4^- are 179 and 240 pm [36], respectively. The large ClO_4^- anions can occupy more lattice space to make the framework denser, exhibiting higher tolerance toward lattice collapse [37]. In addition, compared to planar NO_3^-, the tetrahedral ClO_4^- can involve more C–H···O hydrogen bonds (Table S3 in Supporting information) with the chains, enhancing the chain-chain interactions. **1** undergoes a two-step mass loss by heating to 500 °C. Two mass losses of 12.1% and 8.0% come up at the ranges of 120–270 °C and 270–430 °C, attributed to the nitrate anions or organic moieties' degradation.

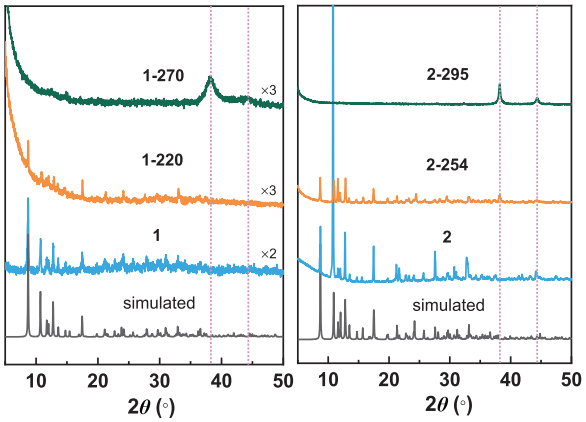

Fig. 3. PXRD diffractograms of **1, 2** and the related thermal treatment samples.

There is no evident plateau in between, and the decomposition continues above 430 °C. Compound **2** shows a stable mass up to 150 °C in agreement with the absence of lattice solvents. The decomposition starts at 150 °C and follows a three-step process. A slight mass loss of 1.1% occurs between 150 °C and 254 °C, followed by two sharply declining mass losses of 3.8% and 12.9% at 254–295 °C and 295–350 °C. The first two mass losses (1.1% and 3.8%) correspond with the stepwise releases of O_2 (calcd. 1.2%) and NO_2 (calcd. 3.5%) from the decomposition of the $AgNO_3$ component. Furthermore, the generation of NO_2 (m/z = 46) was confirmed by the thermogravimetric and mass spectrometric (TG-MS) analyses for **1** and **2** (Fig. S5 in Supporting information). The similar total weight loss (~22.3%) at 500 °C for both **1** and **2** indicates the homologous residual components.

TG analyses of bulk $AgNO_3$ and the mononuclear complex $Co(notpH_3)\cdot 3H_2O$ were also performed in the Ar atmosphere as a comparison (Fig. S4 in Supporting information). The decomposition of $AgNO_3$ (Eq. 1) becomes appreciable around 330 °C and entirely at 470 °C. The ligand decomposition in $Co(notpH_3)\cdot 3H_2O$ occurs at around 287 °C and tends to be stable at 430 °C. The results of TG analyses indicate that (1) the dispersion can reduce the thermal stability of the $AgNO_3$ component; (2) lattice ClO_4^- anions compared to NO_3^- anions can promote the organic moieties' thermal stability.

$$2AgNO_3 \xrightarrow{\Delta} 2Ag + 2NO_2 \uparrow + O_2 \uparrow \quad (1)$$

Insights into the structural transformation during decomposition are provided by powder XRD measurements for selected samples annealing at different temperatures (220 and 270 °C for **1**; 254 and 295 °C for **2**) shown in Fig. 3. The PXRD patterns of **2**–254 remain almost when heating **2** to 254 °C, indicating that the assembly of $Co(notpH_3)$ units does not change and Ag atoms are still embedding in the chains structures. The fitted cell parameters of **2**–254 are similar to those of **2** (Fig. S7 and Table S4 in Supporting information). When the annealing temperature reaches 295 °C, **2** undergoes the secondary weight loss, and the resulting solid **2**–295 becomes a crystalline-amorphous composite. All observed diffraction peaks at 2θ = 38.2°, 44.4° and 64.5° can be assigned to crystalline Ag with cubic (*Fm*-3*m*) lattice (Fig. S6 and Table S1 in Supporting information). For **1**, the diffraction peaks caused by the crystalline H-bonded assembly are still evident after annealing at 220 °C. Furthermore, the PXRD pattern of **1**–270 confirms the generation of crystalline Ag.

The above results indicate that the thermal decomposition reaction of $AgNO_3$ can occur in 1D Co-Ag coordination chains at a temperature below T_d of bulk $AgNO_3$. Also, the decomposition consists of two stages, which are proposed in Fig. 1a. First, the product O_2 releases, and the product NO_2 retains in the coordination chain to bridge two adjacent $\{Co_2Ag_2\}$ units. Next, the bridged NO_2 releases and the collapse of H-bonded networks accompanies the formation of crystalline Ag. It is worth noting that Ag(0) atoms appear in the $\{Co_2Ag_2\}$ units at the first stage. The further magnetic and X-ray absorption fine-structure (XAFS) studies reveal the valence change of Ag atoms during the decomposition.

Magnetic susceptibilities, measured in the temperature range 1.8–300 K under an external field of 1 kOe, reveal a diamagnetic nature for compounds **1** and **2**, in agreement with the presence of a low spin d^6 Co(III) and d^{10} Ag(I) (Fig. S6 in Supporting information). After heating, the resulting samples **1**–220**, 1**–270, **2**–254 and **2**–295 become paramagnetic. The $\chi_M T$ values (per Co_2Ag_2 unit) at 300 K are 1.17 cm^3 K/mol for **1**–220, 7.18 cm^3 K/mol for **1**–270, 0.84 cm^3 K/mol for **2**–254, and 7.41 cm^3 K/mol for **2**–295. The $\chi_M T$ value for **2**–254 is compatible with the spin-only value (0.75 cm^3 K/mol) for the 1/2 (Ag^0)–1/2 (NO_2) spin system. Furthermore, the $\chi_M T$ value for **2**–295 agrees well with the presence of two high spin octahedral Co(II) with a significant orbital contribution. It indicates NO_2 within the chain releases while an undefined Co(II) species produces. X-ray photoelectron spectroscopy (XPS) is applied to analyze the Co(II)/Co(III) on the particle's surface of **2,** **2**–254 and **2**–295 (Fig. S8 in Supporting information). The spectra of **2** and **2**–254 are almost the same, with two peaks at 780.7 and 795.7 eV. While the spectrum of **2**–295 shows the observable satellite features at around 784.1 and 802.2 eV (~3.4 and 6.5 eV above the main peak), indicating the oxidation state of Co(II) [38]. On account of no obvious turning point between the releases of O_2 and NO_2 for **1**, the $\chi_M T$ value for **1**–220 is larger than the spin-only value (0.75 cm^3 K/mol) for the two separated spin-1/2 system. After the release of NO_2, the $\chi_M T$ values for **1**–270 and **2**–295 are almost identical.

The *ex-situ* Ag K-edge XANES spectra of **1** and the samples heated at 100, 150, 180, 200, 220, 240 and 280 °C are given in Fig. 4a, which also shows the spectra of Ag-foil and $AgNO_3$ standards. Edge energy obtained at half-height of the normalized edge-jump could be used to monitor changes in the oxidation state for Ag qualitatively. The edge position of **1** is 25,514.0 eV, identical to that of the $AgNO_3$ standard (25,513.5) and 2 eV lower than that of the Ag-foil standard (25,516.0 eV). For the thermally treated samples of **1**, the edge positions of **1**–100, **1**–150, **1**–180 and **1**–200 are almost the same at 25,514.3 eV, suggesting the Ag oxidation state of +1. Furthermore, the edge positions of **1**–240 and **1**–280 are almost identical at 25,515.6 eV, suggesting the metallic form of Ag. The edge position of **1**–220 is at 25,514.8 eV between the positions of $AgNO_3$ and Ag-foil standards, indicating the mixed-valence (0 and +1) Ag centers.

The EXAFS data of those samples were also analyzed to realize the changes in the coordination sphere of Ag centers after thermal treatment. Shown in Fig. S8 and Fig. 4b are the Ag K-edge k^3-weight $\chi(k)$ data and their Fourier-transformed (FT) data, respectively. It is found that **1,** **1**–100, **1**–150, **1**–180 and **1**–200 present an FT peak located at the identical position of around 1.7 Å, corresponding to the nearest Ag-O coordination. While for **1**–220, two FT peaks at 1.7 and 2.0 Å appear on the Ag-O region, indicating two kinds of local atomic arrangements around the Ag centers. This structural change might arise from the reducing half Ag(I) ions to Ag(0) atoms in the chain. The additional structural parameters fitting for two kinds of Ag coordination spheres are unsuccessful due to too many variables. The FT peak at 2.5 Å with significantly increased intensity is observed for **1**–240, **1**–280 and the Ag-foil, corresponding to the agglomeration of Ag atoms *via* Ag-Ag bonds.

In conclusion, we synthesized two 1-D Co-Ag phosphonates containing the $AgNO_3$ component. Under optimal temperature, as expected, not only the thermal decomposition of $AgNO_3$ can produce metallic Ag in CPs, but the single Ag atoms are stabilized in

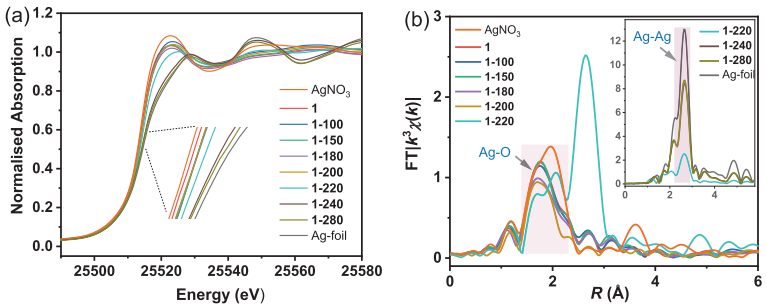

Fig. 4. (a) Ag K-edge XANES spectra and (b) Fourier transformed space (R space) at Ag K-edge of **1** and its thermally treated samples. The spectra of Ag-foil and $AgNO_3$ were recorded as a comparison.

the chain *via* phosphonate-Ag coordination. However, the atomically dispersed metallic Ag is embedded in a dense structure and inactive. Further work is trying to disperse single atoms of metallic silver in porous CPs or CP nanosheets using this method.

Declaration of competing interest

The authors declare that they have no known competing financial interests or personal relationships that could have appeared to influence the work reported in this paper.

Acknowledgments

Financial support by the National Natural Science Foundation of China (Nos. 21671098, 21731003) and the Fundamental Research Funds for the Central Universities (Nos. 14380151, 14380206) is acknowledged. We thank Professor Xizhang Wang at Nanjing University for the valuable discussion. Beam time at Shanghai Synchrotron Radiation Facility (SSRF) is acknowledged.

Supplementary materials

Supplementary material associated with this article can be found, in the online version, at doi:10.1016/j.cclet.2021.10.091.

References

[1] H. Furukawa, K.E. Cordova, M. O'Keeffe, O.M. Yaghi, Science 341 (2013) 1230444.
[2] S. Kitagawa, R. Kitaura, S. Noro, Angew. Chem. Int. Ed. 43 (2004) 2334–2375.
[3] J.P. Zhang, X.M. Chen, Metal-Organic Frameworks for Photonics Applications, in: B. Chen, G. Qian (Eds.), Structure and Bonding, Springer, 2014, pp. 1–26.
[4] A.W. Peters, Z.Y. Li, O.K. Farha, J.T. Hupp, ACS Nano 9 (2015) 8484–8490.
[5] T. He, S.M. Chen, B. Ni, et al., Angew. Chem. Int. Ed. 57 (2018) 3493–3498.
[6] T.T. Sun, L.B. Xu, D.S. Wang, Y.D. Li, Nano Res. 12 (2019) 2067–2080.
[7] J.X. Han, J.J. Bian, C.W. Sun, Research (2020) 9512763.
[8] S.L. Yang, J. Zhang, L. Peng, et al., Chem. Sci. 11 (2020) 10991–10997.
[9] D.D. Ma, Q.L. Zhu, Coord. Chem. Rev. 422 (2020) 213483.
[10] C.C. Hou, H.F. Wang, C.X. Li, Q. Xu, Energy Environ. Sci. 13 (2020) 1658–1693.
[11] H.Z. Yang, R. Shi, L. Shang, T.R. Zhang, Small Struct. 2 (2021) 2100007.
[12] Y.J. Li, S.Y. Lin, D.D. Wang, et al., Adv. Mater. 32 (2020) 1906722.
[13] J.R. Yang, W.H. Li, D.S. Wang, Y.D. Li, Small Struct. 2 (2021) 2000051.
[14] J.S. Wu, Z. Li, H.X. Tan, et al., Anal. Chem. 93 (2021) 1732–1739.
[15] Y.B. Zhao, N. Kornienko, Z. Liu, et al., J. Am. Chem. Soc. 137 (2015) 2199–2202.
[16] J.W. Ren, T.C. Jen, Coord. Chem. Rev. 430 (2021) 213734.
[17] T. Luo, S. Shakya, P. Mittal, et al., Int. J. Pharm. 584 (2020) 119407.
[18] Z.P. Chen, S. Pronkin, T.P. Fellinger, et al., ACS Nano 10 (2016) 3166–3175.
[19] X.H. Jiang, L.S. Zhang, H.Y. Liu, et al., Angew. Chem. Int. Ed. 59 (2020) 23112–23116.
[20] X.X. Yao, W.J. Zhang, J.L. Huang, et al., Appl. Catal. A 601 (2020) 117647.
[21] F.L. Wang, Y.F. Wang, Y.Y. Li, et al., Dalton Trans. 47 (2018) 6924–6933.
[22] M.A. Wahab, C.M. Hasan, Z.A. Alothman, M.S.A. Hossain, J. Hazard. Mater. 408 (2021) 124919.
[23] Y.X. Chen, D.M. Tang, Z.W. Huang, et al., Nat. Commun. 12 (2021) 1191.
[24] S.S. Bao, M.F. Qin, L.M. Zheng, Chem. Commun. 56 (2020) 12090–12108.
[25] S.S. Bao, Y. Liao, Y.H. Su, et al., Angew. Chem. Int. Ed. 50 (2011) 5504–5508.
[26] S.S. Bao, K. Otsubo, J.M. Taylor, et al., J. Am. Chem. Soc. 136 (2014) 9292–9295.
[27] S.B. Liu, S.S. Bao, L.M. Zheng, Dalton Trans. 49 (2020) 3758–3765.
[28] S.S. Bao, N.Z. Li, J.M. Taylor, et al., Chem. Mater. 27 (2015) 8116–8125.
[29] Y. Hou, H.J. Pang, C.J. Gómez-Garciá, et al., Inorg. Chem. 58 (2019) 16028–16039.
[30] S.S. Batsanov, Inorg. Mater. 37 (2001) 871–885.
[31] T.T. Yeh, J.Y. Wu, Y.S. Wen, et al., Dalton Trans. (2005) 656–658.
[32] X.T. Wang, X.H. Wang, Z.M. Wang, et al., Inorg. Chem. 48 (2009) 1301–1308.
[33] Y.Y. Yu, P.Z. Huang, Y.Z. Wang, et al., Chin. Chem. Lett. 32 (2021) 3558–3561.
[34] H. Li, C.W. Hu, J. Solid State Chem. 177 (2004) 4501–4507.
[35] D.W. Fu, J.X. Gao, W.H. He, et al., Angew. Chem. Int. Ed. 59 (2020) 17477–17481.
[36] H.D.B. Jenkins, K.P. Thakur, J. Chem. Edu. 56 (1979) 576–577.
[37] M.L. Ding, X.C. Cai, H.L. Jiang, Chem. Sci. 10 (2019) 10209–10230.
[38] St.G. Christoskova, M. Stoyanova, M. Georgieva, et al., Mater. Chem. Phys. 60 (1999) 39–43.